



Screening and optimization of the most influencing factors during the photodegradation of Rhodamine B by zinc oxide photocatalyst: application of Plackett–Burman and central composite designs

Sabrina Aziri¹ · Hakima Bozetine¹ · Smail Meziane¹ · Djaouida Allam¹ · Nabila Berkane¹ · Rezika Bakri¹ · Abdeltif Amrane²

Received: 15 February 2024 / Accepted: 29 April 2024 / Published online: 30 May 2024
© Akadémiai Kiadó, Budapest, Hungary 2024

Abstract

Zinc oxide (ZnO) powder synthesized by microwave irradiation method was used as photocatalyst for optimization of the photocatalytic degradation conditions of Rhodamine B dye under UV irradiation. The structural, morphological and optical characterizations of elaborated ZnO were performed by infrared spectroscopy, UV spectroscopy, X-ray diffraction, scanning electron microscopy, energy dispersive X-ray spectroscopy and Bruner-Emmett-Teller surface area analysis. Plackett–Burman design was first used to evaluate the effects of five parameters (initial dye concentration, contact time, lamp height, material dose and initial pH of the solution) on the photocatalytic degradation efficiency of the dye. The obtained results showed that contact time and initial dye concentration are the parameters that influence the photocatalytic degradation yield. The effects in decreasing order of the five factors were as follows: contact time (46.597) > initial dye concentration (– 29.149) > lamp height (– 8.419) > ZnO mass (7.263) > pH (1.0072). Subsequently, a central composite design for the two influencing parameters was performed to optimize the dye photodegradation process. It was found that the effect of contact time on the photodegradation efficiency was the highest, followed by the effect of initial dye concentration, and the interactions between initial dye concentration and contact time. The predicted and the experimental values were found to be in good agreement; the coefficient of determination value 0.996 and the adjusted coefficient of determination value 0.993 indicated that the model was significant. First-order kinetic model successfully fitted the experimental data. The synthesized photocatalyst was found to be photostable during at least five regeneration cycles.

Keyword Zinc oxide · Rhodamine B · Photodegradation · Plackett and Burman · Central composite design

Introduction

Textile dyes are among the most dangerous organic pollutants as they threaten water quality and the environment. They are used in many industrial sectors such as food, cosmetics, clinics, and particularly in the textile industries. The release of colored effluents into the environment is aesthetically unpleasant. These effluents inhibit light penetration, retard photosynthesis, inhibit the growth of aquatic life, and adversely affect the quality of receiving waterways [1, 2]. Approximately 1–20% of the total global dye production is lost during the dyeing process and is released in the textile effluents [3]. Community health is seriously threatened by exposure to these chemicals. Contact with organic dyes can result in a number of negative health effects, including dermatitis, ulceration of the skin and mucous membranes, perforation of the nasal septum, severe respiratory tract irritation, vomiting, hemorrhage, pain, and sharp diarrhea [4].

Among the various synthetic dyes, Rhodamine B (Rh-B) stands out; it is frequently used in the textile industry to color cotton, silk, wool, and leather because of its excellent stability. Due to its widespread application, this dye is constantly present in aquatic resources [5, 6]. According to some studies, if this organic compound is disposed of improperly, it can have teratogenic and carcinogenic effects on organisms [7].

Therefore, efficient and environmentally friendly methods for the treatment of wastewater containing dyes are urgently required. Different techniques including biological and physicochemical techniques have been employed to remove dyes from wastewater. The aerobic and anaerobic biological treatment processes have certain limitations. Particularly, these techniques take a long time for operation and are highly sensitive to experimental conditions [8]. It has been also shown that a large number of organic compounds, particularly those that are hazardous or refractory, are extremely resistant to biological degradation [9, 10]. Anaerobic oxidation, flocculation, adsorption, precipitation, reverse osmosis, and coagulation are examples of physicochemical processes that are not effective because these techniques employ chemicals which produce secondary pollution [11].

As an alternative, advanced oxidation processes (AOPs) are considered potential and promising techniques for the treatment of dye contaminated wastewater. The AOPs are more effective for the removal of organic pollutants in comparison to other chemical techniques. The AOPs include photolysis, Fenton processes, electrochemical oxidations and both homogeneous and heterogeneous chemical and photochemical processes. Since Honda and Fujishima [12] carried out the first photo-catalyzed AOP based on titanium-oxide (TiO_2) in 1972, heterogeneous photocatalysis using semiconductors oxides as photocatalysts had gained many concerns. These photocatalysis are irradiated with UV, near-UV, or visible light at ambient temperature and pressure and in the presence of oxygen. The heterogeneous photocatalysis process occurs with the absorption of light radiation of an energy ($h\nu$) greater than or equal to the bandgap energy of the photocatalyst ($h\nu \geq E_g$) [13]. Photon absorption causes the excitation and transfer

of electrons (e^-) from the valence band to the conduction band, leading to the generation of holes (h^+) in the valence band. The second step is the separation and migration of charge carriers (e^- and h^+) to the catalyst surface. The highly reactive electrons and holes on the photocatalyst surface tend to perform oxidation and reduction reactions to produce hydroxyl radicals ($\cdot\text{OH}$) and superoxide anion radicals (O_2^-). This technique has been successfully applied for wastewater treatment, and it is suitable to completely degrade organic pollutants [14]. Zinc oxide (ZnO) is a semiconductor widely used as a photocatalyst due to its low cost of procurement and good catalytic properties, wide band gap (3.37 eV), UV light sensitivity, and lack of toxicity [15, 16]. These fascinating properties explain its large application in heterogeneous photocatalysis.

The efficiency of dye photodegradation depends on a multitude of variables, including dye concentration, solution pH, catalyst dose, light intensity, and intermediate species [11]. The concentration of dyes greatly affects the photocatalytic performances. With an increase in initial concentration from 100 to 400 mg/L, Adeel et al. found that photodegradation of methyl orange by Co–ZnO decreased from 77 to 42% [17]. The pH of dye solution also significantly affects the photodegradation performance. Siddique et al. have studied the effect of pH on Rhodamine B dye photodegradation over bismuth ferrite catalyst and they reported that the highest photodegradation was at neutral pH [18]. The degradation efficiency of pollutants increases with the increase of catalyst dose. Lu et al. have investigated the effect of the amount of CdS/graphene catalyst on the photodegradation of Rhodamine B dye, they observed that the increase of catalyst dose from 200 to 1800 mg/L increased the photodegradation percentage from 49 to 86% [19]. The radiation source is a very important ingredient in the photocatalytic process and photon flux is a key factor in photochemical reactions [20]. Light intensity plays an important role in the degradation of pollutants due to its efficient role in the formation of large quantities of $\cdot\text{OH}$ radical [21]. Consequently, an increase in light intensity should lead to an increase in reaction rates [22]. However, as light intensity increases, its effect on reaction kinetics decreases so that its impact becomes negligible at high intensities [23].

Conventional experimental methodology involves setting the level of all variables except one, and measuring the system's response to different values of that variable, which requires the experimenter to carry out a large number of experiments. To overcome this problem, Fisher [24, 25] proposed the design-of-experiments method for the first time, allowing to study several factors at the same time. The principle of experimental design is to vary the levels of all factors at the same time in each experiment. This greatly reduces the number of experiments to be carried out, and increases the number of factors studied. The design-of-experiments method aims to determine a relationship between the response, which is the physical quantity being studied, and the factors, which are physical quantities that can be modified by the experimenter and are expected to have an impact on variations in the response. There are currently a large number of different experimental designs, which can be divided into two main categories: designs to study the effects of parameters like Plackett and Burman design and designs for adjusting parameters to reach an optimum like Box-Behnken, central composite and Taguchi designs.

In this study, zinc oxide synthesized by microwave method was used as photocatalyst for the degradation of Rhodamine B under UV irradiation. First, the factors influencing the photodegradation process were determined using Plackett and Burman design (PBD). Then, a central composite design (CCD) was carried out to optimize the most significant variables influencing the photodegradation of Rhodamine B.

Materials and methods

Synthesis of ZnO powder

ZnO nanoparticles were prepared by a microwave-assisted method. In a 400 mL beaker, a solution of 0.1 M zinc acetate dihydrate ($\text{Zn}(\text{CH}_3\text{COO})_2 \cdot 2\text{H}_2\text{O}$) was prepared. A solution of 1 M NaOH was added dropwise under constant stirring until a pH equal to 8 was obtained, then left under stirring for 5 min. After formation of a white precipitate, it was transferred to a 500 mL crystallizer and then irradiated with a Whirlpool domestic microwave at 680 Watts for 6 min. The resulting white precipitate was cooled to room temperature, centrifuged, washed with distilled water and ethanol several times and dried in an oven at 80 °C for 24 h.

The obtained ZnO powder was characterized by Fourier transform infrared (FTIR), UV–visible, X-ray diffraction (XRD), scanning electron microscopy (SEM), energy dispersive X-ray spectroscopy (EDS) and Bruner–Emmett–Teller (BET).

Rhodamine B photodegradation experiments and analysis

The photodegradation experiments were performed in a 400 mL cylindrical reactor. Stirring of the photocatalyst-dye mixture was provided by magnetic stirring. Before irradiation, the suspension was stirred in the dark for 30 min to establish the adsorption–desorption equilibrium. Irradiation was performed using a UV lamp of 365 nm wavelength and a power of 125 W (Bailey UVHPR125).

For each experiment, a given amount of ZnO powder is contacted with 50 ml of a Rhodamine B solution of known pH and initial concentration. The desired initial pH of the solution was adjusted by adding a solution of hydrochloric acid HCl (0.1 M) or sodium hydroxide NaOH (0.1 M). The stirring speed was kept constant during all the photodegradation process. After a well-defined contact time, the mixture was centrifuged, and the supernatant was analyzed by a Shimadzu UV-1601PC spectrophotometer (Japan) to determine the residual Rhodamine B concentration.

The degradation efficiency noted R was calculated using the following equation:

$$R(\%) = \frac{(A_0 - A_t)}{A_0} \quad (1)$$

Here A_0 is the initial absorbance and A_t is the absorbance of Rh-B solution after a certain irradiation time.

Table 1 Factors studied and their levels in PBD

Factors	Symbols	Levels	
		- 1	+ 1
pH of the solution	$X_1 = \text{pH}$	2	6
Photocatalyst mass (g)	$X_2 = m$	0.05	0.1
Initial dye concentration (mg/L)	$X_3 = C_0$	5	20
Contact time (min)	$X_4 = t_c$	10	50
UV Lamp height (cm)	$X_5 = h$	15	25

Table 2 Levels of factors in central composite design

Factors	Symbols	Levels				
		$-\alpha (-1.414)$	- 1	0	+ 1	$+\alpha (+1.414)$
Initial dye concentration (mg/L)	$X_1 = C_0$	5.43	7.5	12.5	17.5	19.57
Contact time (min)	$X_2 = t_c$	8.79	15	30	45	51.21

Design of experiments methodology

Plackett and Burman

Plackett and Burman design is a particular type of fractional factorial design, which is principally used to screen and evaluate the important parameters that appear to influence the selected response with a reduced number of experiments. The five parameters studied in this study along with their range of variation are reported in Table 1.

The PBD is based on a first-order model (Eq. 2) that does not describe any interaction between the parameters [26]:

$$R(\%) = \beta_0 + \beta_1 x_i \tag{2}$$

Here R is the experimental response (%), β_0 is the model intercept, β_i is the linear coefficient and x_i is the level of the independent variable.

The parameters with probability value (p value) below 0.05, i.e., more than 95% confidence level of all intervals, are thought about to have a significant effect on the photodegradation of Rhodamine B by zinc oxide, and by using CCD and response surface methodology (RSM), the significant independent parameters are optimized.

Central composite design

According to PBD results, a central composite design was performed in order to optimize the most significant variables (t_c et C_0) that influenced the

photodegradation of Rhodamine B by zinc oxide. Table 2 shows the two significant independent variables and their levels.

The mathematical relationship between the independent variables was expressed with a second-order polynomial model given in the equation below:

$$R(\%) = \beta_0 + \beta_1x_1 + \beta_2x_2 + \beta_{11}x_1^2 + \beta_{22}x_2^2 + \beta_{12}x_1x_2 \quad (3)$$

Here R is the predicted response, β_0 is the intercept term, β_1 and β_2 are the linear coefficients, β_{11} and β_{22} are the quadratic coefficients, β_{12} is the interaction coefficient, x_1 and x_2 represents the independent variables.

The fitness of the polynomial model equation was evaluated by the coefficient of determination R^2 and adjusted R^2 . The response was analyzed using analysis of variance (ANOVA) based on the p value with 95% of confidence level.

Modde 6 software was used for developing PBD for the screening of independent variables and for designing a CCD and RSM for optimization of significant independent parameters.

Photodegradation kinetics

The kinetic degradation of Rhodamine B in the presence of ZnO was realized by fixing the parameters at the center of the study domain (pH 4, $m_{\text{ZnO}}=0.075$ g, $[\text{Rh-B}]_0=12.5$ mg/L, $h=20$ cm, $V_{\text{solution}}=50$ mL). The results were analyzed using a first order kinetic model, this model assumes that the rate is proportional to the residual concentration of the pollutant in the solution. This model is given by the following equation:

$$r_1 = -\frac{d[c]}{dt} = k_{\text{app}} \times [c]^1 \quad (4)$$

Here r_1 is the catalytic degradation rate ($\text{mg L}^{-1}\text{min}^{-1}$), k_{app} is the apparent degradation constant (min^{-1}), $[c]$ is the concentration of Rhodamine B (mg L^{-1}) and “t” is the reaction time (min).

Results and discussion

Characterization

Fourier transform infrared spectrum was collected using an IR Affinity-1S Shimadzu spectrometer in the region of 400–4000 cm^{-1} (Fig. 1a). The elongation vibrations of (-OH) group of adsorbed water molecules have been found at 3834, 3742 and 3480 cm^{-1} [27, 28]. The band located at 2345 cm^{-1} is due to the atmospheric CO_2 present in the instrument. Peaks at 1512 and 1651 cm^{-1} are attributed to the symmetric and asymmetric stretching of carboxylic groups of acetate attached to ZnO nanoparticles [29]. The absorption peaks at 663 and 478 cm^{-1} are associated to Zn–O stretching vibrations [30].

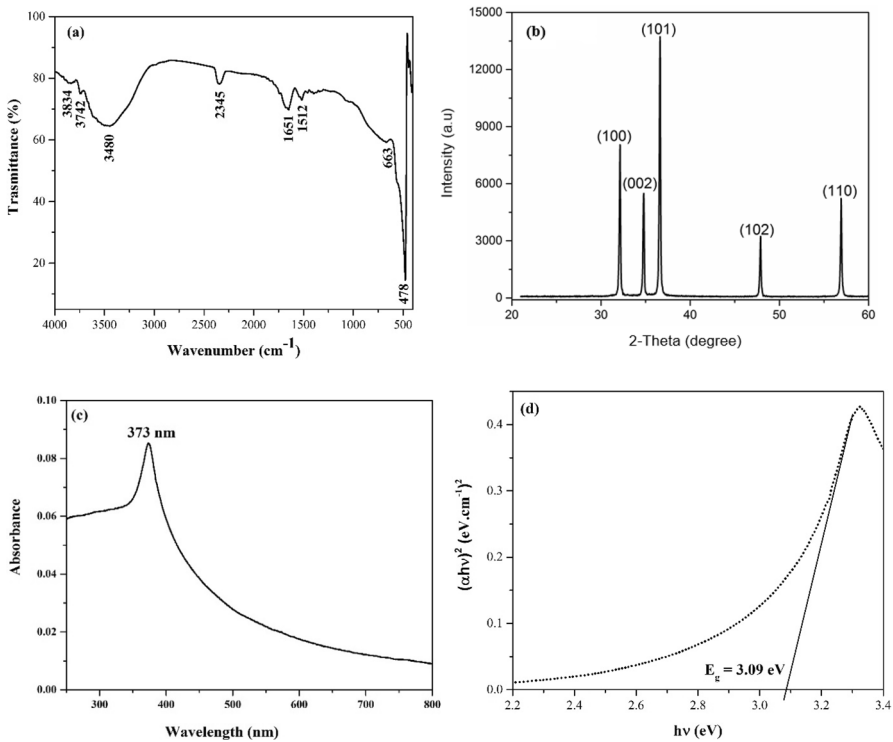


Fig. 1 (a) Infrared spectrum of ZnO powder, (b) X-ray diffraction spectrum of ZnO, (c) UV–visible absorption spectrum of ZnO nanostructures, (d) band gap of ZnO nanostructure using Tauc equation

The resulting solid was characterized using X-ray powder diffraction (XRD) (Rigaku D/Max-kA X-ray diffractometer, $\text{CuK}\alpha$ radiation). XRD pattern of ZnO is shown in Fig. 1b. The observed peaks can be indexed to wurtzite ZnO. As clearly show in this figure all the diffraction peaks corresponding to (100), (002), (101), (102) and (110) planes can be assigned to hexagonal wurtzite structured ZnO according to the norm (JCPDS card No. 01- 079 - 0207). The spectrum is in accordance with those reported for ZnO prepared using different methods [31, 32].

The UV–Visible absorption spectrum was performed to study the optical properties of ZnO which play an important role in photocatalysis. It was recorded by Shimadzu UV-1601C spectrophotometer in the wavelength range 200–800 nm. Fig. 1c shows that ZnO powder presents an absorption peak in the UV region at 373 nm assigned to the intrinsic gap absorption of ZnO. Except for the defined absorption peak; no other peaks were observed, confirming that the synthesized product consisted only of ZnO [33].

The band gap energy of the catalyst was calculated using the Tauc equation:

$$(\alpha h\nu)^n = B(h\nu - E_g) \quad (5)$$

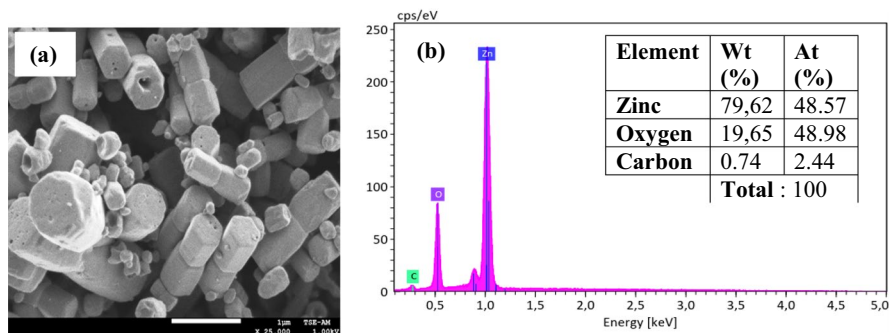


Fig. 2 (a) Scanning electron microscopy image of ZnO NPs, (b) Energy dispersive X-ray spectrum of ZnO sample

Table 3 Surface properties of ZnO nanoparticles

Properties	Values
Specific surface area (S_{BET}) (m^2/g)	1.936
Total pore volume (cm^3/g)	0.012
Pore diameter (\AA)	20.710

Here “ E_g ” is the band gap energy, B is a constant, ν is the frequency of the incident radiation, h is the Planck’s constant, α is the absorption coefficient and n is determined by the type of optical transition of a semiconductor (n equal to 2 for direct transition band gaps). Band gap energy of ZnO was determined by extrapolating the linear region of $(\alpha h\nu)^2$ vs $h\nu$ on the x -axis [34]. Fig. 1d shows that the gap energy of ZnO is 3.09 eV, namely slightly lower than the value of bulk ZnO which is 3.37 eV [35]. This can be attributed to the presence of oxygen vacancies or/and defects at the surface of ZnO nanocrystals [36, 37]. A similar result was found by Cao et al. [38] and Sarma et al. [39].

The morphology and the surface elemental composition of the photocatalyst were obtained using a JEOL 6700 F scanning electronic microscopy equipped with an energy dispersive X-ray analyzer. The SEM image of the synthesized material is shown in Fig. 2a. The results revealed that the ZnO powder can be clearly distinguished as individual particles with no agglomeration. The figure shows micro-sized hexagonal ZnO rods, which had an average length of 0.1–100 μm and diameter of 0.1–0.5 μm . The EDX spectrum (Fig. 2b) demonstrates that the catalyst consisted mainly of zinc, oxygen and residual carbon. The table in Fig. 2b gives the percentage of each constituent element.

Textural properties were obtained by nitrogen adsorption–desorption isotherms at room temperature on a Nova 2000e. Specific surface area was determined according to the Bruner–Emmett–Teller (BET) method. According to Fig. S1, the isotherm can be identified as type IV (IUPAC classification), which reflected the mesoporous nature of the material [16] and corresponding to a capillary

Table 4 Experimental results of photodegradation of Rhodamine B by ZnO obtained with PBD

Essay	Parameters in coded values					Parameters in real values					R _{exp} (%)	R _{cal} (%)
	pH	m	C ₀	t _c	h	pH	m	C ₀	t _c	h		
1	+1	+1	+1	-1	+1	6	0.1	20	10	25	13.55	15.02
2	-1	+1	+1	+1	-1	2	0.1	20	50	15	75.06	69.03
3	-1	-1	+1	+1	+1	2	0.05	20	50	25	47.31	53.34
4	+1	-1	-1	+1	+1	6	0.05	5	50	25	89.53	83.49
5	-1	+1	-1	-1	+1	2	0.1	5	10	25	44.63	43.16
6	+1	-1	+1	-1	-1	6	0.05	20	10	15	17.64	16.17
7	+1	+1	-1	+1	-1	6	0.1	5	50	15	93.15	99.18
8	-1	-1	-1	-1	-1	2	0.05	5	10	15	42.85	44.32
9	0	0	0	0	0	4	0.075	12.5	30	20	49.75	52.96
10	0	0	0	0	0	4	0.075	12.5	30	20	52.08	52.96
11	0	0	0	0	0	4	0.075	12.5	30	20	51.41	52.96

Table 5 Statistical analysis of the experimental results of Rh-B degradation obtained with PBD

Factors	Coefficients	Standard error	p value
Constant	52.7649	1.7619	7.79 × 10 ⁻⁷
pH	0.5036	2.0661	0.8171
m	3.6315	2.0661	0.1391
C	- 14.5749	2.0661	0.00088
tc	23.2986	2.0661	9.58 × 10 ⁻⁵
h	- 4.2098	2.0661	0.09717

condensation [40]. The specific surface area, total pore volume and pore diameter of ZnO are given in Table 3.

Determination of the influencing parameters

The response studied was the degradation efficiency of Rhodamine B by ZnO. The experimental results obtained are reported in Table 4. In the studied experimental domain, the degradation efficiency varied from 13.55 to 93.15%. This large variation indicates that at least one factor had an influence on Rhodamine B photodegradation by ZnO.

Statistical analysis of results is given in Table 5, it includes model coefficients, standard error and probability value for each factor. The coefficients of pH, mass and contact time were positive. Therefore, their influence was positive on the degradation of Rhodamine B. The coefficients of the concentration and the height of the lamp were negative. Consequently, these parameters influenced negatively the process of photodegradation.

For a 5% risk, contact time and initial dye concentration were the factors that influence the photodegradation of Rhodamine B by ZnO. The contact time with a probability of $9.58 \cdot 10^{-5}$ was the most influential factor. By choosing a risk of 10%, the height of the lamp negatively influenced the photodegradation process.

The graphical representation of the effects of the factors is given by Fig. 3. As shown in this figure, the effect of the contact time on the photodegradation efficiency (46.597) was the highest. It was followed by the effects of initial dye concentration (− 29.149), lamp height (− 8.419), ZnO mass (7.263) and pH (1.0072).

The mathematical model as a function of all factors in coded variables is written as:

$$R = 52,7649 + 0,5036X_1 + 3,6315X_2 - 14,5749X_3 + 23,2986X_4 - 4,20981X_5 \quad (6)$$

with a relatively high coefficient of determination, equal to 0.974.

Central composite design (CCD)

The above Plackett and Burman design (PBD) study showed that the factors influencing the photodegradation process of Rhodamine B by ZnO were the initial dye concentration and contact time. A central composite design (CCD) was then considered to investigate the individual and interaction effects of these factors on the response. The coded and real values of the initial dye concentration and the contact time of the central composite design matrix in 11 experimental runs are presented in Table 6.

The results of the statistical analysis are summarized in Table 7. The p values of the model terms can be used to control the significance of the terms; they are significant when their p values are less than 0.05. As seen from this table, initial

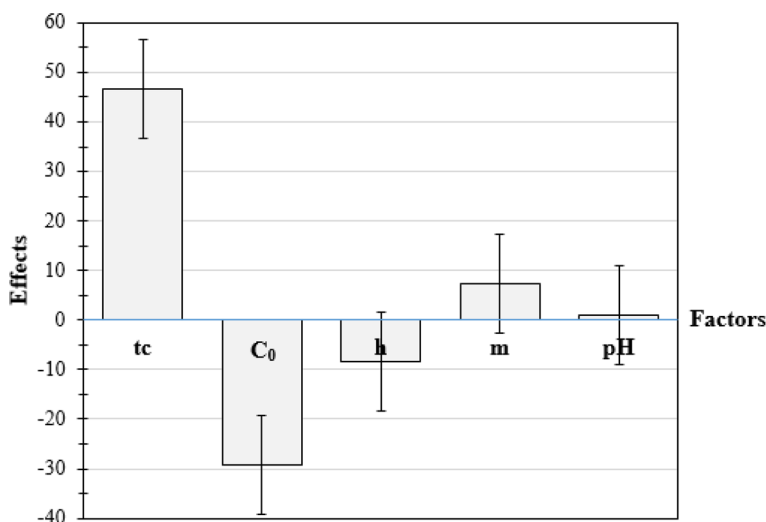


Fig. 3 Plackett and Burman design/ Graphical study of the effects

Table 6 Experimental design and obtained results with CCD

Essay	Coded values		Real values		R _{exp} (%)	R _{cal} (%)	Residual
	C	tc	C	tc			
1	- 1	- 1	7.5	15	44.64	44.63	0.01
2	1	- 1	17.5	15	31.97	30.79	1.18
3	- 1	1	7.5	45	86.42	85.91	0.51
4	1	1	17.5	45	51.95	50.27	1.68
5	- 1.414	0	5.43	30	75.66	75.68	- 0.02
6	1.414	0	19.57	30	39.02	40.70	- 1.67
7	0	- 1.414	12.5	8.79	25.64	26.13	- 0.49
8	0	1.414	12.5	51.21	67.88	69.08	- 1.20
9	0	0	12.5	30	49.75	51.08	- 1.33
10	0	0	12.5	30	52.08	51.08	1.00
11	0	0	12.5	30	51.41	51.08	0.33

Table 7 Statistical analysis of the experimental results obtained with CCD

Factors	Coefficients	Standard error	p value
Constant	51.0805	0.8905	3.04696 × 10 ⁻⁸
C ₀	- 12.3692	0.5454	3.098 × 10 ⁻⁶
tc	15.1880	0.5454	1.11768 × 10 ⁻⁶
C ₀ *C ₀	3.5570	0.6492	0.00276132
t _c *t _c	- 1.7377	0.6492	0.0439995
C ₀ *t _c	- 5.4488	0.7712	0.000878513

dye concentration, contact time, the quadratic terms of initial dye concentration and contact time, and the interaction C₀-t_c had significant effects on the photodegradation of Rhodamine B dye by ZnO under UV irradiation. The coefficients of contact time and quadratic term of initial dye concentration were positive, showing a positive impact on the degradation of Rhodamine B. On the other hand, the coefficients of the initial concentration, quadratic term of contact time and the interaction C₀-t_c were negative, showing a negative influence on the degradation process.

The value of the correlation coefficient value (R²=0.996) indicated the high correlation between the experimental results and predicted values. The adj-R² value was found to be 0.993 and this value was found to be compatible with the R² value.

The second order quadratic equation which represented the Rhodamine dye removal (R) as a function of initial dye concentration (x₁) and contact time (x₂) in coded variables can be written as:

$$R = 51.0805 - 12.3692x_1 + 15.188x_2 + 3.55697x_1^2 - 1.73768x_2^2 - 5.44875x_1x_2 \tag{7}$$

The graphical representation of the effects of the factors and interactions is displayed in Fig. S2. This figure clearly shows that the effect of contact time (30.376) on photodegradation efficiency was the highest, followed by the effects of initial Rhodamine B concentration (-24.738), C_0 - t_c interaction (-10.897), C_0 - C_0 interaction (7.114) and t_c - t_c interaction (-3.475). This result confirms the previous finding, i.e. photodegradation efficiency increases with increasing irradiation time and decreases with increasing initial dye concentration of Rhodamine B. It could be concluded that treatment of samples containing low concentrations of Rhodamine B necessitates shorter irradiation times and, thus, lower energy. At high Rh-B concentration levels, the activity is less because more molecules blanket the photocatalyst's active sites, interrupting light intensity, and consequently decreasing photodegradation efficiency [41, 42].

The model adequacy can be judged using diagnostic graphs such as the predicted versus experimental values plot. Fig. S3 shows the graph of observed data for the removal efficiency of the Rhodamine B dye versus the values predicted using the model. The coefficient of determination was equal to 0.996, indicating a linear relationship between the predicted and observed values.

The results of the experimental design studied for the degradation of Rhodamine B by ZnO yielded the response surfaces and contours are shown in Fig. 4. The exploitation of the graphs allows the visualization and determination of the optimal conditions for the degradation in the defined study domain. By setting the level of an independent variable at the center of the experimental domain, it is possible to follow the evolution of the other two variables and their influence on the degradation performance. This figure illustrates the effect of the initial concentration of Rhodamine B and the contact time on the photodegradation efficiency. It clearly shows that the optimal yields were obtained for high values of contact time and low values of concentration. It can be seen that the higher the contact time, the better the photodegradation yield obtained. In contrast to the contact time, the higher the initial dye

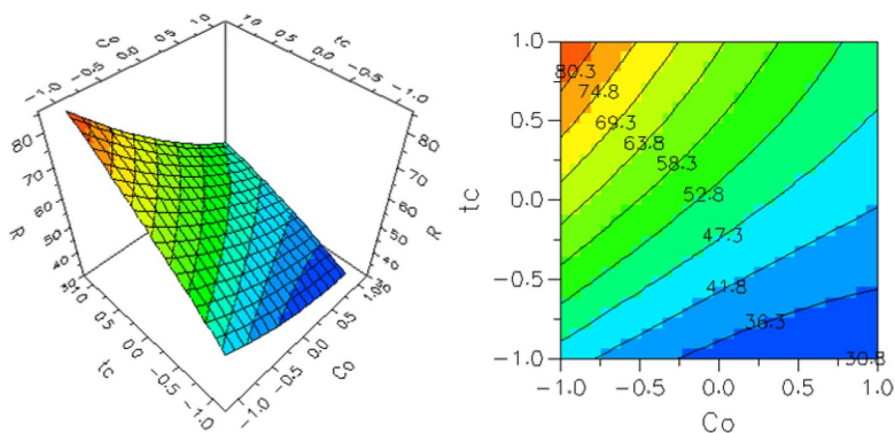


Fig. 4 Contours and response surfaces of Rh-B photodegradation by ZnO: Effect of initial Rhodamine B concentration and contact time (pH 4, $m_{\text{ZnO}}=0.075$ g, $h=20$ cm, $V_{\text{solution}}=50$ mL)

concentration, the lower the yield. The maximum dye removal was found at the lowest dye concentration of 7.5 mg/L and contact time of 45 min.

The decrease of the performance of the photocatalytic degradation of Rhodamine dye by ZnO with the increase of the initial concentration can be attributed to the decrease of the ratio of the active sites of the photocatalyst to the dye molecules, to the absorption of light rather than its penetration to the surface of the catalyst and to the decrease of the ratio of $\cdot\text{OH}$ radicals to dye molecules [11].

Kinetic study

The evolution of the UV–visible absorption spectrum of Rhodamine B as a function of irradiation time with UV light in the presence of the ZnO catalyst is shown in Fig. S4. It can be seen that the intensity of the peak at 554 nm characterizing the Rhodamine B dye decreased with the irradiation time.

Fig. 5 shows the results of photolysis and photocatalysis of Rh-B. It shows that the discoloration by photolysis under UV light was low, with only 9% removal after 180 min; while, in the presence of the photocatalyst suspension, Rhodamine B was almost completely removed, with about 99% discoloration.

The dye degradation rate was determined by fitting the experimental data by the pseudo-first order kinetic model. The value of the rate constant was determined using nonlinear regression (Fig. 6). As shown in this figure, a single exponential decay function fits well the experimental data points of C_t against t with R^2 value equal to 0.995, indicating the validity of the pseudo-first order kinetic to the photodegradation of Rh-B by ZnO nanoparticles. This result indicates that the rate of heterogeneous photocatalytic degradation of Rh-B is proportional to the fraction of the catalyst surface covered by the synthetic dye [43]. The apparent

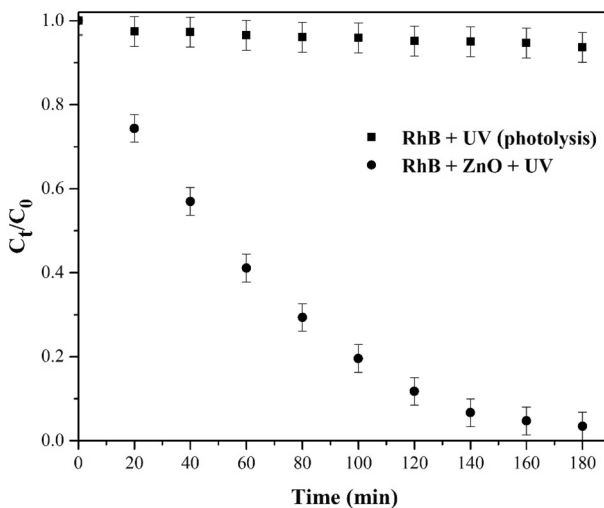


Fig. 5 Rhodamine B degradation as a function of irradiation time in the absence and presence of ZnO (pH 4, $m_{\text{ZnO}} = 0.15$ g, $[\text{Rh-B}]_0 = 12.5$ mg/L, $h = 20$ cm, $V_{\text{solution}} = 100$ mL)

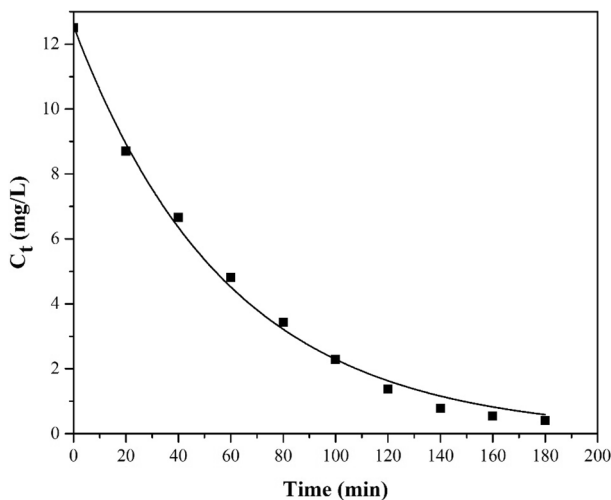


Fig. 6 The non-Linear plot for the pseudo-first kinetic model for the Rhodamine B degradation by ZnO (pH 4, $m_{(\text{ZnO})} = 0.15\text{g}$, $[\text{Rh-B}]_0 = 12.5\text{ mg/L}$, $h = 20\text{ cm}$, $V_{\text{solution}} = 100\text{ mL}$)

degradation constant (k_{app}) was found to be 0.017 min^{-1} . This result is in agreement with the related literature dealing with the photodegradation of Rhodamine B by different catalysts [32, 44, 45].

The photocatalytic reaction typically involves photoexcitation, charge separation and migration, and surface redox reactions [46]. The reactive species generated during photocatalyst illumination are holes (h^+), hydroxyl radicals ($\cdot\text{OH}$), superoxide radicals ($\text{O}_2^{\cdot-}$) and electrons (e^-). To understand the mechanism of Rh-B degradation by ZnO under UV irradiation, it is necessary to detect the reactive species that play a major role in the photocatalytic degradation process. To achieve this, we added tert-butyl alcohol (TBA), ascorbic acid (AA), ammonium oxalate (AO) and potassium dichromate ($\text{K}_2\text{Cr}_2\text{O}_7$) to scavenge hydroxyl radicals, superoxide radicals, holes and electrons [47, 48]. For comparison purpose, another experiment was performed without scavenger (NS).

Fig. 7 displays the photocatalytic results when four different scavengers were added. The figure shows that 99% degradation of Rh-B was found in the absence of any scavenger, while 90% degradation was found with OA. This indicates that holes played a minor role in the degradation process. It was also observed that by using $\text{K}_2\text{Cr}_2\text{O}_7$, AA and TBA as scavengers, the photocatalytic efficiency decreased from 99% (no scavenger) to 76.72% (e^-), 65.22% ($\text{O}_2^{\cdot-}$) and 51.43% ($\cdot\text{OH}$). Hence, it is concluded that electrons, hydroxyl and superoxide radicals contribute significantly in the photodegradation process. Furthermore, $\cdot\text{OH}$ is the predominant reactive specie since significant decrease in photocatalytic activity was obtained when TBA was used as a scavenger.

The possible mechanism for degradation of Rh-B by ZnO can be proposed as follows:

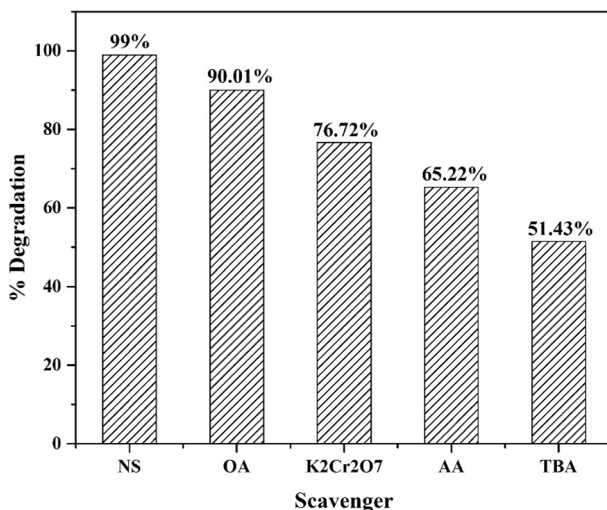
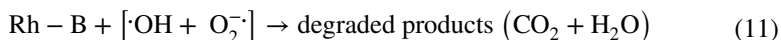
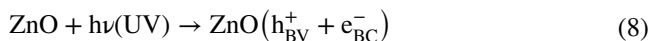


Fig. 7 Effect of various scavengers: TBA (0.65 mM), AA (1 mM), AO (1mM) and K₂Cr₂O₇ (1 mM) on the degradation of Rh-B by ZnO under UV light irradiation (pH 4, $m_{\text{ZnO}}=0.15$ g, $[\text{Rh-B}]_0=12.5$ mg/L, $t_{\text{irradiation}}=180$ min, $h=20$ cm, $V_{\text{solution}}=100$ mL)



Photocatalyst stability

The economic efficiency of a photocatalytic reaction is highly dependent on the number of times a catalyst can be reused without significant loss of photocatalytic efficiency [49]. Catalyst stability is also an important factor in photocatalysis; regeneration of nanoparticles is important for their environmental and industrial applications [50].

To explore the reusability of the synthesized ZnO photocatalyst, photodegradation experiments were repeated several times and the results are shown in Fig. 8. In these tests, the same catalyst was reused several times with Rhodamine B. The experimental results show that the photocatalytic activity of ZnO did not decrease significantly after five successive degradation cycles, showing the stability of the material during the photodegradation process.

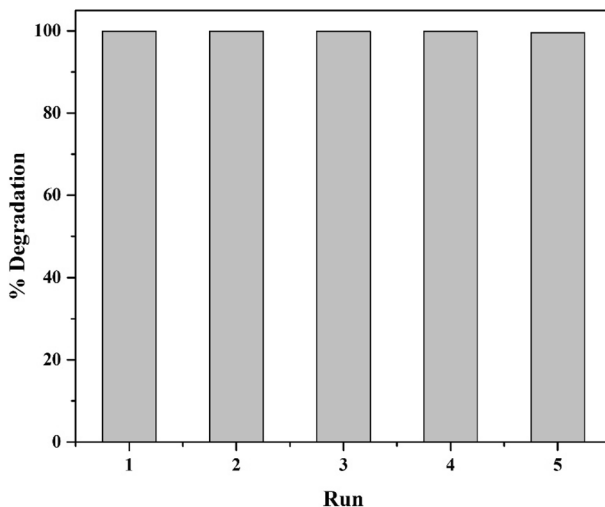


Fig. 8 Removal efficiencies obtained after successive recycling of ZnO (pH 4, $m_{\text{ZnO}}=0.15$ g, $[\text{Rh-B}]_0=12.5$ mg/L, $t_{\text{irradiation}}=180$ min, $h=20$ cm, $V_{\text{solution}}=100$ mL)

Conclusion

In this work, the photocatalytic degradation of a textile dye, Rhodamine B, was investigated using as semiconductor zinc oxide synthesized by the microwave method. The formation of pure ZnO was confirmed by XRD, FTIR, EDX and UV–vis spectroscopy. The screening of five factors including initial dye concentration, contact time, lamp height, material dose and initial pH of the solution by Plackett and Burman’s design showed that the initial dye concentration and the contact time had a significant influence on the photodegradation process. The application of a central composite design showed that the interaction of initial dye concentration and contact time had a weak effect compared to the effects of contact time and initial dye concentration. The degradation efficiency, based on the coded factor variables (x_1 for initial dye concentration and x_2 for contact time), can be expressed by the following equation:

$$R = 51.0805 - 12.3692x_1 + 15.188x_2 + 3.55697x_1^2 - 1.73768x_2^2 - 5.44875x_1x_2$$

The photodegradation kinetic of Rhodamine B by ZnO was accurately described by the pseudo–first order model. ZnO nanoparticles were successfully recycled over five cycles, showing its stability during the photodegradation process.

Supplementary Information The online version contains supplementary material available at <https://doi.org/10.1007/s11144-024-02641-x>.

Acknowledgements The authors would like to express their gratitude and appreciation to the Director for his kind permission to do this project work at Laboratory of Applied Chemistry and Chemical Engineering, Faculty of Science, University Mouloud Mammeri of Tizi-Ouzou, Algeria.

Data availability The datasets generated and/or analysed during the current study are presented in this manuscript and supplementary information file.

Declarations

Competing interest The authors did not receive support from any organization for the submitted work.

References

1. Garg VK, Kumar R, Gupta R (2004) Removal of malachite green dye from aqueous solution by adsorption using agro-industry waste: a case study of *Prosopis cineraria*. *Dyes Pigments* 62(1):1–10. <https://doi.org/10.1016/j.dyepig.2003.10.016>
2. Padmesh TVN, Vijayaraghavan K, Sekaran G, Velan M (2006) Biosorption of Acid Blue 15 using fresh water macroalga *Azolla filiculoides*: Batch and column studies. *Dyes Pigments* 71:77–82. <https://doi.org/10.1016/j.dyepig.2005.06.003>
3. Akpan UG, Hameed BH (2009) Parameters affecting the photocatalytic degradation of dyes using TiO₂ based photocatalysts: a review. *J Hazard Mater* 170(2–3):520–529. <https://doi.org/10.1016/j.jhazmat.2009.05.039>
4. Nguyen VN, Tran DT, Nguyen MT, Le TTT, Ha MN, Nguyen MV, Pham TD (2018) Enhanced photocatalytic degradation of methyl orange using ZnO/graphene oxide nanocomposites. *Res Chem Intermed* 44:3081–3095. <https://doi.org/10.1007/s11164-018-3294-3>
5. Carneiro JO, Samantilleke AP, Parpot P, Fernandes F, Pastor M, Correia A, Chivanga Barros AA, Luís EA, Teixeira V (2016) Visible light induced enhanced photocatalytic degradation of industrial effluents (Rhodamine B) in aqueous media using TiO₂ nanoparticles. *J Nanomater*. <https://doi.org/10.1155/2016/4396175>
6. Dhanavel S, Nivethaa EAK, Dhanapal K, Gupta VK, Narayanan V, Stephen A (2016) α -MoO₃/polyaniline composite for effective scavenging of Rhodamine B, Congo red and textile dye effluent. *RSC Adv* 6(34):28871–28886. <https://doi.org/10.1039/c6ra02576e>
7. Rangel EM, de Melo CCN, Machado FM (2019) Ceramic foam decorated with ZnO for photodegradation of Rhodamine B dye. *Bol Soc Esp Ceram V* 58(3):134–140. <https://doi.org/10.1016/j.bsecv.2018.10.002>
8. Garcia BB, Lourinho G, Romano P, Brito PSD (2020) Photocatalytic degradation of swine wastewater on aqueous TiO₂ suspensions: optimization and modeling via Box-Behnken design. *Heliyon*. <https://doi.org/10.1016/j.heliyon.2020.e03293>
9. Khan FI, Husain T, Hejazi R (2004) An overview and analysis of site remediation technologies. *J Environ Manag* 71(2):95–122. <https://doi.org/10.1016/j.jenvman.2004.02.003>
10. Yeung AT, Gu YY (2011) A review on techniques to enhance electrochemical remediation of contaminated soils. *J Hazard Mater* 195:11–29. <https://doi.org/10.1016/j.jhazmat.2011.08.047>
11. Saeed M, Muneer M, Haq AU, Akram N (2022) Photocatalysis: an effective tool for photodegradation of dyes—a review. *Environ Sci Pollut Res*. <https://doi.org/10.1007/s11356-021-16389-7>
12. Fujishima A, Honda K (1972) Electrochemical photolysis of water at a semiconductor electrode. *Nature* 238(5358):37–38. <https://doi.org/10.1038/238037a0>
13. Zhang L, Mohamed HH, Dillert R, Bahnemann D (2012) Kinetics and mechanisms of charge transfer processes in photocatalytic systems: a review. *J Photochem Photobiol* 13(4):263–276. <https://doi.org/10.1016/j.jphotochemrev.2012.07.002>
14. Loddò V, Bellardita M, Camera-Roda G, Parrino F, Palmisano L (2018) Heterogeneous photocatalysis: a promising advanced oxidation process. In: *Current trends and future developments on (bio-) membranes*, pp 1–43. <https://doi.org/10.1016/B978-0-12-813549-5.00001-3>
15. Boughelout A, Macaluso R, Kechouane M, Trari M (2020) Photocatalysis of rhodamine B and methyl orange degradation under solar light on ZnO and Cu₂O thin films. *React Kinet Mech Cat* 129:1115–1130. <https://doi.org/10.1007/s1144-020-01741-8>
16. Garg R, Gupta R, Singh N, Bansal A (2021) Characterization and performance evaluation of synthesized ZnO nanoflowers, nanorods, and their hybrid nanocomposites with graphene oxide

- for degradation of Orange G. *Environ Sci Pollut Res* 28(40):57009–57029. <https://doi.org/10.1007/s11356-021-14511-3>
17. Adeel M, Saeed M, Khan I, Muneer M, Akram N (2021) Synthesis and characterization of Co–ZnO and evaluation of its photocatalytic activity for photodegradation of methyl orange. *ACS Omega* 6(2):1426–1435. <https://doi.org/10.1021/acsomega.0c05092>
 18. Siddique M, Khan NM, Saeed M (2019) Photocatalytic activity of bismuth ferrite nanoparticles synthesized via sol-gel route. *Z Phys Chem* 233(5):595–607. <https://doi.org/10.1515/zpch-2018-1225>
 19. Lü W, Chen J, Wu Y, Duan L, Yang Y, Ge X (2014) Graphene-enhanced visible-light photocatalysis of large-sized CdS particles for wastewater treatment. *Nanoscale Res Lett* 9:1–7. <https://doi.org/10.1186/1556-276X-9-148>
 20. Zeghioud H, Khellaf N, Djelal H, Amrane A, Bouhelassa M (2016) Photocatalytic reactors dedicated to the degradation of hazardous organic pollutants: kinetics, mechanistic aspects, and design—a review. *Chem Eng Commun* 203(11):1415–1431. <https://doi.org/10.1080/00986445.2016.1202243>
 21. Behnajady MA, Modirshahla N, Daneshvar N, Rabbani M (2007) Photocatalytic degradation of an azo dye in a tubular continuous-flow photoreactor with immobilized TiO₂ on glass plates. *Chem Eng J* 127(1–3):167–176. <https://doi.org/10.1016/j.cej.2006.09.013>
 22. Guo J, Dong C, Zhang J, Lan Y (2015) Biogenic synthetic schwertmannite photocatalytic degradation of acid orange 7 (AO7) assisted by citric acid. *Sep Purif Technol* 143:27–31. <https://doi.org/10.1016/j.seppur.2015.01.018>
 23. Faramarzpour M, Vossoughi M, Borghei M (2009) Photocatalytic degradation of furfural by titania nanoparticles in a floating-bed photoreactor. *Chem Eng J* 146(1):79–85. <https://doi.org/10.1016/j.cej.2008.05.033>
 24. Fisher RA (1936) Design of experiments. *Br Med J* 1(3923):554–554. <https://doi.org/10.1136/bmj.1.3923.554-a>
 25. Fisher RA (1992) Statistical methods for research workers. In: *Breakthroughs in statistics*. Springer, New York, pp 66–70. https://doi.org/10.1007/978-1-4612-4380-9_6
 26. Plackett RL, Burman JP (1946) The design of optimum multifactorial experiments. *Biometrika* 33(4):305–325. <https://doi.org/10.2307/2332195>
 27. Chauhan DS, Gopal CSA, Kumar D, Mahato N, Quraishi MA, Cho MH (2018) Microwave induced facile synthesis and characterization of ZnO nanoparticles as efficient antibacterial agents. *Mater Discov* 11:19–25. <https://doi.org/10.1016/j.md.2018.05.001>
 28. Khan M, Alam MS, Ahmed SF (2023) Effect of nickel incorporation on structural and optical properties of zinc oxide thin films deposited by RF/DC sputtering technique. *Mater Phys Mech* 51:19–32. https://doi.org/10.18149/MPM.5112023_3
 29. Panda NR, Sahu D, Acharya BS, Nayak P (2015) High UV absorption efficiency of nanocrystalline ZnO synthesized by ultrasound assisted wet chemical method. *Curr Appl Phys* 15(3):389–396. <https://doi.org/10.1016/j.cap.2015.01.014>
 30. Rao LS, Rao TV, Naheed S, Rao PV (2018) Structural and optical properties of zinc magnesium oxide nanoparticles synthesized by chemical co-precipitation. *Mater Chem Phys* 203:133–140. <https://doi.org/10.1016/j.matchemphys.2017.09.048>
 31. Srujana S, Bhagat D (2022) Chemical-based synthesis of ZnO nanoparticles and their applications in agriculture. *Nanotechnol Environ Eng* 7(1):269–275. <https://doi.org/10.1007/s41204-022-00224-6>
 32. Jothibas M, Paulson E, Mathivanan A, Srinivasan S, Kannan KS (2023) Biomolecules influences on the physiochemical characteristics of ZnO nanoparticles and its enhanced photocatalysis under solar irradiation. *Nanotechnol Environ Eng*. <https://doi.org/10.1007/s41204-023-00310-3>
 33. Tripathy N, Ahmad R, Kuk H, Lee DH, Hahn YB, Khang G (2016) Rapid methyl orange degradation using porous ZnO spheres photocatalyst. *J Photochem Photobiol B Biol* 161:312–317. <https://doi.org/10.1016/j.jphotobiol.2016.06.003>
 34. Adegoke KA, Iqbal M, Louis H, Bello OS (2019) Synthesis, characterization and application of CdS/ZnO nanorod heterostructure for the photodegradation of Rhodamine B dye. *Mater Sci Energy Technol* 2(2):329–336. <https://doi.org/10.1016/j.mset.2019.02.008>
 35. Chitra M, Mangamma G, Uthayarani K, Neelakandeswari N, Girija EK (2020) Band gap engineering in ZnO based nanocomposites. *Phys E: Low Dimens Syst Nanostures* 119:113969. <https://doi.org/10.1016/j.physe.2020.113969>

36. Chanu LA, Singh WJ, Singh KJ, Devi KN (2019) Effect of operational parameters on the photocatalytic degradation of Methylene blue dye solution using manganese doped ZnO nanoparticles. *Results Phys* 12:1230–1237. <https://doi.org/10.1016/j.rinp.2018.12.089>
37. Sharma D, Jha R (2017) Analysis of structural, optical and magnetic properties of Fe/Co co-doped ZnO nanocrystals. *Ceram Int* 43(11):8488–8496. <https://doi.org/10.1016/j.ceramint.2017.03.201>
38. Cao W, Chen L, Qi Z (2015) Microwave-assisted synthesis of Ag/Ag₂SO₄/ZnO nanostructures for efficient visible-light-driven photocatalysis. *J Mol Catal A: Chem* 401:81–89. <https://doi.org/10.1016/j.molcata.2015.02.023>
39. Sarma B, Sarma BK (2017) Fabrication of Ag/ZnO heterostructure and the role of surface coverage of ZnO microrods by Ag nanoparticles on the photophysical and photocatalytic properties of the metal-semiconductor system. *App Surf Sci* 410:557–565. <https://doi.org/10.1016/j.apsusc.2017.03.154>
40. Nandi P, Das D (2019) Photocatalytic degradation of Rhodamine-B dye by stable ZnO nanostructures with different calcination temperature induced defects. *Appl Surf Sci* 465:546–556. <https://doi.org/10.1016/j.apsusc.2018.09.193>
41. Nadim AH, Al-Ghobashy MA, Nebsen M, Shehata MA (2015) Optimization of photocatalytic degradation of meloxicam using titanium dioxide nanoparticles: application to pharmaceutical wastewater analysis, treatment, and cleaning validation. *Environ Sci Pollut Res* 22:15516–15525. <https://doi.org/10.1007/s11356-015-4713-2>
42. Elumalai N, Prabhu S, Selvaraj M, Silambarasan A, Navaneethan M, Harish S, Ramu P, Ramesh R (2022) Enhanced photocatalytic activity of ZnO hexagonal tube/r-GO composite on degradation of organic aqueous pollutant and study of charge transport properties. *Chemosphere* 291:132782. <https://doi.org/10.1016/j.chemosphere.2021.132782>
43. Kamaluddin MR, Zamri NII, Kusriani E, Prihandini WW, Mahadi AH, Usman A (2021) Photocatalytic activity of kaolin–titania composites to degrade methylene blue under UV light irradiation; kinetics, mechanism and thermodynamics. *React Kinet Mech Cat* 133(1):517–529. <https://doi.org/10.1007/s11444-021-01986-x>
44. Dai WL, Xu H, Yang LX, Luo XB, Tu XM, Luo Y (2015) Ultrasonic-assisted facile synthesis of plasmonic Ag@AgCl cuboids with high visible light photocatalytic performance for Rhodamine B degradation. *React Kinet Mech Cat* 115:773–786. <https://doi.org/10.1007/s11444-015-0870-z>
45. Cheng J, Zhao S, Gao W, Jiang P, Li R (2017) Au/Fe₃O₄@TiO₂ hollow nanospheres as efficient catalysts for the reduction of 4-nitrophenol and photocatalytic degradation of rhodamine B. *React Kinet Mech Cat* 121:797–810. <https://doi.org/10.1007/s11444-017-1185-z>
46. Chen X, Wu Z, Liu D, Gao Z (2017) Preparation of ZnO photocatalyst for the efficient and rapid photocatalytic degradation of azo dyes. *Nanoscale Res Lett* 12:1–10. <https://doi.org/10.1186/s11671-017-1904-4>
47. Su J, Zhu L, Geng P, Chen G (2016) Self-assembly graphitic carbon nitride quantum dots anchored on TiO₂ nanotube arrays: an efficient heterojunction for pollutants degradation under solar light. *J Hazard Mater* 316:159–168. <https://doi.org/10.1016/j.jhazmat.2016.05.004>
48. Akir S, Hamdi A, Addad A, Coffinier Y, Boukherroub R, Omrani AD (2017) Facile synthesis of carbon-ZnO nanocomposite with enhanced visible light photocatalytic performance. *App Surf Sci* 400:461–470. <https://doi.org/10.1016/j.apsusc.2016.12.212>
49. Chakrabarti S, Dutta BK (2004) Photocatalytic degradation of model textile dyes in wastewater using ZnO as semiconductor catalyst. *J Hazard Mater* 112(3):269–278. <https://doi.org/10.1016/j.jhazmat.2004.05.013>
50. Jadhav SA, Somvanshi SB, Khedkar MV, Patade SR, Jadhav KM (2020) Magneto-structural and photocatalytic behavior of mixed Ni–Zn nano-spinel ferrites: visible light-enabled active photo-degradation of Rhodamine B. *J Mater Sci Electron* 31(14):11352–11365. <https://doi.org/10.1007/s10854-020-03684-1>

Publisher's Note Springer Nature remains neutral with regard to jurisdictional claims in published maps and institutional affiliations.

Springer Nature or its licensor (e.g. a society or other partner) holds exclusive rights to this article under a publishing agreement with the author(s) or other rightsholder(s); author self-archiving of the accepted manuscript version of this article is solely governed by the terms of such publishing agreement and applicable law.

Authors and Affiliations

Sabrina Aziri¹  · Hakima Bozetine¹ · Smail Meziane¹ · Djaouida Allam¹ · Nabila Berkane¹ · Rezika Bakri¹ · Abdeltif Amrane²

✉ Sabrina Aziri
sabrina.aziri@ummto.dz

¹ Laboratory of Applied Chemistry and Chemical Engineering, Faculty of Science, University Mouloud Mammeri of Tizi-Ouzou, Tizi-Ouzou, Algeria

² Univ Rennes, Ecole Nationale Supérieure de Chimie de Rennes, CNRS, ISCR–UMR 6226, 35000 Rennes, France